Capillarity

Vol. 14, No. 2, p. 35-52, 2025

Original article

Saturation-functions models in CO_2-brine system: A comparative study

Mohsen Faramarzi[1,2], S. Mostafa Tabatabaei[1], Behnam Sedaee[1,3]*, Nikta Attari[4], S. Amirali Panahi[1]

[1]*Institute of Petroleum Engineering, School of Chemical Engineering, College of Engineering, University of Tehran, Tehran 1417935840, Iran*

[2]*Department of Chemical Engineering, Université Laval, Québec G1V 0A8, Canada*

[3]*Department of Chemical & Petroleum Engineering , Schulich School Of Engineering, University of Calgary, Calgary T2N 1N4, Canada*

[4]*Department of Mechanical Engineering, University of British Colombia, Vancouver V6T 1Z4, Canada*

Keywords:
Capillary pressure
relative permeability
carbon capture and storage
CO_2 geo-sequestration
CO_2-brine
saturation functions

Cited as:
Faramarzi, M., Tabatabaei, S. M., Sedaee, B., Attari, N., Panahi, S. A. Saturation-functions models in CO_2-brine system: A comparative study. Capillarity, 2025, 14(2): 35-52.
https://doi.org/10.46690/capi.2025.02.01

Abstract:
CO_2 injections into deep saline aquifers create a multiphase flow system within the porous media. In this context, relative permeability and capillary pressure, as saturation functions, are key parameters that control flow dynamics, simulation accuracy, and operational decisions. Since various models have been proposed for the saturation functions, this study aims to assess the existing models and investigate which model performs best under different circumstances. To this end, we first gathered a comprehensive data set to evaluate the existing models. Following that, the nonlinear fitting of experimental data was used to obtain the parameters of each model. Finally, the root-mean-square error and correlation coefficients were used to assess the accuracy of the fit. Based on the results of capillary pressure analysis, the models can be classified into two main categories. The first category includes models with power-law behavior suitable for homogeneous formations (single curvature), such as Brooks-Corey, Li-Horne, Lambda, Thomeer, Leverett J-function, and modified J-function models. The second category includes Van Genuchten, Kosugi, Skelt-Harison, Johnson, and Jing-Van Wunnik, which can be applied to homogeneous and heterogeneous formations (capture more than one curvature). Regarding relative permeability, the L.E.T., Chierici, Van Genuchten, and Corey models exhibit comparable performance across all scenarios. Corey offers simplicity with minimal parameters, while Van Genuchten provides more adaptability for complex data sets with more physically based parameters.

1. Introduction

The idea of Carbon Capture and Storage has been advocated as one potential approach for reducing CO_2 emissions and addressing global warming (Falkowski et al., 2000; Jia et al., 2018). CO_2 sequestration is commonly used to target different geological formations such as deep saline aquifers, depleted hydrocarbon reservoirs, and coal seams (Pini et al., 2012; Wang et al., 2013; Raza et al., 2019; Hashemi et al., 2020; Bakhshian et al., 2020; Faramarzi-Palangar et al., 2021a). The potential of deep saline aquifers to store substantial amounts of CO_2 makes them the most important CO_2 sinks among all the geological formations (Choi et al., 2013; Dai et al., 2018). The injection of CO_2 into deep saline aquifers constitutes a drainage process wherein the

Yandy Scientific Press

*Corresponding author.
E-mail address: mohsen.faramarzi-palangar.1@ulaval.ca (M. Faramarzi); mosi.tabatabaei@gmail.com (S. M. Tabatabaei); sedaee@ut.ac.ir (B. Sedaee); nikta.attari@ubc.ca (N. Attari); samiralipanahi@ut.ac.ir (S. A. Panahi).

Received October 28, 2024; revised December 5, 2024; accepted January 22, 2025; available online January 29, 2025.

nonwetting phase (CO_2) displaces the wetting phase (brine), resulting in a two-phase flow system (CO_2-brine). Multiphase flow involving two or more immiscible phases within a porous medium is complicated to understand; therefore, features such as relative permeability, displacement process, and saturation distribution are essential to explore using numerical models and core scale experiments (Bennion and Bachu, 2008b; Silin et al., 2011; Berg et al., 2013; Pini et al., 2013; Alizadeh and Piri, 2014; Bakhshian and Hosseini, 2019; Bakhshian et al., 2020; Faramarzi-Palangar et al., 2021a, 2021b).

The most significant parameters for defining multiphase flow behavior in porous media are relative permeability and capillary pressure. To assess the reservoir performance and make the optimal operational decisions, these parameters must be precisely analyzed (Li, 2010; Zhang and Yang, 2013). Capillary pressure and relative permeability curves are typically expressed as functions of local fluid saturation, microscopic porous media characteristics, and pore-scale flow dynamics (Tsakiroglou et al., 2003; Zhang and Yang, 2013; Faramarzi-Palangar et al., 2021b).

Four techniques are usually employed to determine a capillary pressure curve: (I) Mercury injection, (II) restored-state (the porous diaphragm), (III) centrifugal, and (IV) vapor desorption. In comparison to other methods, mercury injection is frequent and less expensive (Brown, 1951; Greder et al., 1997; Newsham et al., 2004). Obtaining relative permeability data is also challenging in some circumstances, such as remarkably low-permeable rocks and atypical fluid systems with significant phase transition and mass transfer between two phases. This is why numerous mathematical models have been presented to calculate relative permeability from capillary pressure data (Li and Horne, 2001; Li, 2004, 2010). Purcell (1949) devised a method for determining relative permeability based on the pore size distribution acquired from mercury injection capillary pressure curves. According to Gates and Lietz (1950), this technique is used to measure two-phase relative permeabilities. As a result, it is better to study the capillary pressure and relative permeability simultaneously (Sun and Mohanty, 2003; Zhang and Yang, 2013). There have been several models developed for capillary pressure and relative permeability in the literature (Bennion and Bachu, 2006, 2008a, 2008b; Pentland et al., 2011; Akbarabadi and Piri, 2013). Among these, the Van Genuchten (1980) and Brooks and Corey (1966) models are the most commonly used, with their applicability primarily determined by the heterogeneity of the porous media and physical parameters such as pore size distribution. The Van Genuchten model is generally applied to more heterogeneous media with a broader range of pore sizes, whereas the Brooks-Corey model is typically suited to media with more uniform pore size distributions (Oostrom et al., 2016, Ren et al., 2016). The Brooks-Corey model (Brooks and Corey, 1966) is also well-known for determining relative permeability, and like Purcell's model, it uses capillary pressure for its calculations (Li and Horne, 2006; Yu and Archer, 2019).

One of the most critical complications in CO_2 storage is the absence of relative permeability and capillary pressure data for CO_2-brine, and thus the majority of capillary pressure data have been obtained by converting mercury injection capillary pressure data (Imbus et al., 2006; Liu et al., 2010; Berg et al., 2013; Zhang and Yang, 2013). The Mercury injection capillary pressure (MICP) method, which uses small rock samples, is a frequent approach for testing the capillary pressure (P_c)-water saturation (S_w) relationships. Pentland et al. (2011) stated that there is considerable agreement across the mercury air, oil-brine, and CO_2-brine datasets; however, some other researchers believe that MICP data do not accurately represent reservoir flow conditions (Christoffersen and Whitson, 1995; Pini et al., 2012) as the assumptions underlying the application of the Young-Laplace equation for converting data from the mercury-air system to the CO_2-water system have not yet been validated. The accuracy of converted data is not comparable to that of direct CO_2-brine data (Pini et al., 2012; Al-Menhali et al., 2015; Iglauer et al., 2015). However, using the MICP data was a problem that earlier studies had overlooked.

CO_2-brine flow characterization requires a significant investment of time and money; therefore, data scarcity is a significant problem. There have been a few studies on CO_2-brine systems. Oostrom et al. (2016) assessed six relative permeability models for two radial injection scenarios, using data from four well-characterized sandstone types: Berea, Paaratte, Tuscaloosa, and Mt. Simon. Their analysis revealed that the endpoint power-law model produced exceptionally low, uniform gas saturation outside the dry-out zone in the Tuscaloosa sandstone. This outcome was attributed to the rapid decline in aqueous phase relative permeability. Ren et al. (2016) also evaluated the accuracy of five capillary pressure models by converting mercury-injection data from 13 sets of experimental data from different shales in a gas-water system. The Van Genuchten and Kosugi models outperformed the others, while the modified J-function, Brooks and Corey, and Li-Horne models underperformed.

As mentioned earlier, the lack of relative permeability and capillary pressure data in the CO_2-brine system due to challenges in running experiments, time, and cost is a significant issue. On the other hand, these kinds of data are crucial in studies. Thus, we attempted to collect direct CO_2-brine published data, creating a data bank. The unique aspect of the collected data set is that it includes a wide range of formations (sandstone, shale, and carbonate), as well as different pressure and temperature conditions, rock properties, and measurement techniques such as steady state and unsteady state methodologies. In addition, this study reviews the eleven capillary pressure and six relative permeability models. Considering the data diversity and models, the main objective of this research is to suggest the best capillary pressure and relative permeability model for different circumstances. Thus, we expect that the results of this study will be helpful for the environmental and petroleum industries. Engineers will also be able to use the best models in their specific cases under study. Section 2 reviews the models for capillary pressure and relative permeability, and then discusses the collected data and its preprocessing. Section 3 indicates the results, and finally, Section 4 summarizes this study.

2. Method of investigation

There have been several empirical and theoretical models developed to fit or predict capillary pressure and relative permeability. One or more fitting parameters are included in these models to characterize the relative permeability or capillary pressure curve. On the collected data, we applied some of the most commonly used models for predicting capillary pressure and relative permeability to evaluate and compare them. Sections 2.1 and 2.2 introduce the capillary pressure and relative permeability models, followed by Section 2.3 which describes the experimental data. It was necessary to make some corrections to the experimental data before the curve fitting process. Therefore, Section 2.4 discusses the corrections made in this study.

2.1 Capillary pressure models

The J-function is the first semi-empirical relation to enduring time that was proposed by Leverett (1941). The J-function shows how rocks with the same lithology but different physical properties could be described by a single dimensionless function that normalizes capillary pressure curves by considering absolute permeability and porosity in the form of hydraulic radius ($\sqrt{k/\phi}$) (Gao et al., 2014):

$$J_{(S_w)} = \frac{c_J P_c}{\sigma}\sqrt{\frac{k}{\phi}} \tag{1}$$

where P_c is capillary pressure (KPa), σ is surface tension (mN/N), k, and ϕ are permeability (mD) and porosity (fraction), respectively. c_J in this formula, is for unit conversion. A fractal model to characterize the pore structure of lithology was proposed based on the existing J-function and fractal geometry theory (Goda and Behrenbruch, 2011). However, capillary pressure theories suggest that the Leverett J-function (LJF) should also be a function of irreducible water saturation, tortuosity, and pore size distribution. As a result, the LJF should only be used to scale capillary pressure in formations in which the pore size distribution and irreducible water saturation are equal (Sarwaruddin et al., 2001). To incorporate wettability, a revised version of Eq. (1) was employed, which includes contact angle:

$$J_{(S_w)} = \frac{c_{LJF} P_c}{\sigma\cos\theta}\sqrt{\frac{k}{\phi}} \tag{2}$$

$$J_{(S_w)} = A_{LJF} S_w^{B_{LJF}} \tag{3}$$

where θ is contact angle, S_w is wetting phase saturation. A_{LJF}, and B_{LJF} in Eq. (3) are the constants of the model, and c_{LJF} is for unit conversion. As Xu et al. (2016) have shown, B in Eq. (3) is equal to $-1/\lambda$ where λ is defined as the pore size distribution that characterizes the relative frequency of various pore sizes within the medium. This index is typically determined by fitting the model to experimental data, with larger λ values indicating a more uniform pore size distribution and smaller values reflecting a wider range of pore sizes (Brooks and Corey, 1966; Li, 2004). It is possible to predict capillary pressure by combining both Eqs. (2) and (3). For clean sandstone formations, the J-function method was first assumed to be universal. However, various experiments have shown that using the J-function to correlate heterogeneous formations is ineffective. As a result, the approach works best when data from core plugs with comparable pore size distributions are normalized (Goda and Behrenbruch, 2011). It was a commonly used model since the equation formulation is simple and has equal weighting on both petrophysical and capillary pressure (Lalanne and Rebelle, 2014). It is, however, limited to water-wet reservoirs and only works well for homogenous formations (Shi et al., 2018). In recent years, various modified versions of the LJF model according to different purposes were developed. In this study, in addition to the J-function model, the following model was used as the modified J-function model (MJF) (Gdanski et al., 2009):

$$S_e = \left(\frac{\sigma}{a_{2,MJF} P_c}\sqrt{\frac{\phi}{k}}\right)^{1/a_{1,MJF}} \tag{4}$$

where $a_{1,MJF}$ and $a_{2,MJF}$ are the fitting parameters of the model, and S_e is the normalized wetting phase saturation, which could be expressed as follows:

$$S_e = \frac{S_w - S_{wr}}{1 - S_{nwr} - S_{wr}} \tag{5}$$

where S_{wr} and S_{nwr} are wetting and non-wetting residual saturation, respectively. In the case of drainage, S_{nwr} is equal to 0. The key difference between Eqs. (3) and (4) is that Eq. (4) relates to normalized wetting phase saturation (S_e), accounting for residual saturations as defined in Eq. (5), while Eq. (3) uses only wetting phase saturation (S_w) meaning their fitting parameters will not yield the same values.

Thomeer (1960) developed an empirical model to estimate capillary pressure as a function of mercury saturation. The pore geometry factor (F_g) is included in the model to comprise the distribution of heterogeneity in the porous medium (Shi et al., 2018):

$$P_c = P_e \exp\left(\frac{-F_g}{\ln S_{Hg} - \ln S_{Hg_\infty}}\right) \tag{6}$$

where P_e is the entry capillary pressure of the rock sample (KPa), S_{Hg} is the mercury saturation and S_{Hg_∞} is the mercury saturation at an infinite capillary pressure. The original Thomeer equation, or model, was initially developed to characterize mercury injection capillary pressure data. To describe the capillary pressure behavior in a CO_2-brine system or to make it applicable to any two-phase flow system, the equation has been adapted into a generalized form that utilizes S_e, as defined in Eq. (7), as shown below:

$$S_e = 1 - \exp\left(\frac{F_g}{\log P_e - \log P_c}\right) \tag{7}$$

The Thomeer capillary pressure model (T) is approximated by a hyperbola (Goda and Behrenbruch, 2011) and is widely used in the petroleum industry, especially for describing the behavior of drainage curves (Ma and Morrow, 1996).

Corey (1954) proposed a straight-line relationship to characterize the gas-oil capillary pressure. Brooks and Corey (1966) modified this into a well-known model similar to the Thomeer model. The definition of normalized saturation

and the use of different fluid pairs are the main differences between the two models (Behrenbruch et al., 2016). The model is comprised of two fitting parameters including λ and P_e:

$$P_c = P_e S_e^{-1/\lambda} \tag{8}$$

The Brooks-Corey model (BC) is also frequently used in petroleum and other applications (Li, 2004). Nevertheless, recent studies have shown that this model cannot predict well the capillary pressure curve in heterogeneous and fractured porous media (Li, 2004, 2010; Safari et al., 2022), and the model is limited to water-wet reservoirs (Shi et al., 2018). The BC model is mainly applicable to the drainage process (Li, 2010), whereas Li and Horne (2001) (LH) provided the following equation for the imbibition process:

$$P_c = P_{\max}(1 - S_e)^{-1/\lambda} \tag{9}$$

where $P_{\max}$ is the capillary pressure at the residual non-wetting phase saturation. Li (2004) attempted to theoretically develop a more general model of a porous medium based on fractal modeling. When the fractal dimension of a porous medium reaches a limiting value, it can be converted into BC or LH imbibition model (Li, 2010). This demonstrated that the empirically developed BC and LHmodels have a theoretical basis as well (Li, 2010). The more general version of the capillary pressure model is expressed as follows:

$$P_c = P_{\max}(1 - b_{LH} S_e)^{-1/\lambda_d} \tag{10}$$

where b_{LH} is a constant that defines as follows:

$$b_{LH} = 1 - \left(\frac{P_e}{P_{\max}}\right)^{-\lambda_d} \tag{11}$$

where $\lambda_d = 3 - D_f$ and D_f is the fractal dimension, which quantifies the complexity and heterogeneity of the pore structure in the rock sample. The fractal dimension D_f is derived from the relationship between the number of pores and the radius of the pore throats, as described in Li and Horne (2003). A higher D_f value suggests increased heterogeneity in pore size distribution and pore space tortuosity. For example, a D_f nearer to 3 indicates a more complicated and heterogeneous pore structure, whereas a lower D_f indicates a simpler, more homogeneous network. When $D_f < 3$ and $P_{\max}$ tend to infinity, the value of b tends to zero, and then, the equation is reduced to the BC model (Eq. (8)). In the case in which $b_{LH} = 1$, Eq. (10) can be reduced to LH-imbibition. In this comparative study, LH was selected to be considered as Li-Horne (LH) model.

Mualem (1976) developed a model to predict the hydraulic conductivity for unsaturated soil-water retention curves and conductivity saturation. Later, based on Mualem's formula, Van Genuchten, 1980 proposed a rather simpler equation for the hydraulic conductivity of unsaturated soils and it is one of the most frequently used equations (Ren et al., 2016) to predict the relationship between $P_c - S_w$:

$$S_e = \left[1 + (a_{VG} P_c)^{n_{VG}}\right]^{-m_{VG}} \tag{12}$$

The Van Genuchten (VG) model included three independent parameters that could be acquired by fitting experimental data. "a_{VG}" as in physical terms, is inversely proportional to entry pressure (KPa^{-1}) (Ioannidis and Chatzis, 1993; Hopmans et al., 1998). "n_{VG}" denotes the width of pore-size distribution and "m_{VG}" was assumed to equal to $1 - 1/n_{VG}$ (Van Genuchten, 1980; Hopmans et al., 1998). The capillary-pressure curve is often either S-shaped (e.g., the VG model) or convex (e.g., the BC model). The VG model employs a steep slope connecting the endpoint (typically zero) to the plateau region, whereas the BC model includes an entry pressure (Li et al., 2013; Gershenzon et al., 2016).

Several authors have tried to expand the models mentioned above or develop additional capillary pressure models (Ren et al., 2016), such as Kosugi (1996) who derived the following equation based on logarithmic pore size distribution:

$$S_e = \frac{1}{2}\mathrm{erfc}\left(\frac{\ln P_c - \ln P_m}{\sqrt{2} w_K}\right) \tag{13}$$

where P_m is capillary pressure (KPa) related to the median pore radius and w_K is the standard deviation of log-transformed pore size in the Kosugi (K) model.

Jing and Van Wunnik (1998) developed a model that was found to be applicable for various pore structures and rock-fluid systems:

$$P_c = P_c^0 \left[\left(\frac{d_{JV}}{S_w - S_{wr}}\right)^{n_{JV}} + a_{JV}\right] \tag{14}$$

where P_c^0 is a fitting parameter describing the capillary pressure scaling factor, and the other fitting parameters are a_{JV}, d_{JV}, and n_{JV}. Jing and Van Wunnik (JV) model was developed to estimate drainage capillary pressure (Goda and Behrenbruch, 2011).

There are several techniques for calculating saturation height, employing capillary pressure data from numerous core samples at varying depths to derive saturation variation versus height above the free water level. Lambda (Wiltgen et al., 2003) is a saturation height function used in the oil and gas industry, and it is usually utilized in association with petrophysical logs (Nasr, 2015). The lambda function (L) considers that the key predictor for water saturation is the area variance of effective porosity. The model has three fitting parameters, a_L, b_L, and λ which are found by fitting capillary pressure curves:

$$S_w = a_L P_c^{-\lambda} + b_L \tag{15}$$

According to Al-Bulushi et al. (2009), L model is more flexible and complex than the other methods. The Lambda function typically generates excellent saturation height models and closely matches experimental data (Al Waili, 2009).

Another function of saturation height is proposed by Johnson (1987), which is a collective fit in which petrophysical features take precedence over the P_c (Lalanne and Rebelle, 2014). The Johnson (J) model describes water saturation as a function of capillary pressure and permeability:

$$\log S_w = A_J \log k + b_J P_c^{c_J} \tag{16}$$

where A_J, b_J, and c_J are the fitting parameters of the model. it should be mentioned that A_J is a constant slope that is independent of P_c.

Table 1. Summary of the capillary pressure models used in this study, along with their parameter definitions.

Model	Formula	Declaration	Category
J-function (LJF) (Leverett and Lewis, 1941)	$J_{(S_w)} = c_{LJF}\frac{P_c}{\sigma}\sqrt{\frac{k}{\phi}}$; $J_{(S_w)} = A_{LJF}S_w^{B_{LJF}}$	k, ϕ, σ: Physically based input parameters; c_{LJF}, A_{LJF}, B_{LJF}: Fitting parameters	First category (power-law behavior, homogeneous rocks)
Modified J function (MJF) (Gdanski et al., 2009)	$S_e = \left(\frac{\sigma}{a_{2,MJF}P_c}\sqrt{\frac{\phi}{k}}\right)^{1/a_{1,MJF}}$	$a_{1,MJF}$, $a_{2,MJF}$: Fitting parameters; S_e: Its wetting and non-wetting residual saturations can be physically-based fitting parameters	First category
Thomeer (T) (Thomeer, 1960)	$S_e = 1-\exp\left(\frac{F_g}{\log P_e - \log P_c}\right)$	P_e, F_g: Physically based fitting parameters	First category
Brooks and Corey (BC) (Brooks and Corey, 1966)	$P_c = P_e S_e^{-1/\lambda}$	P_e, λ: Physically based fitting parameters	First category
Li and Horne (LH) (Li and Horne, 2001)	$P_c = P_{\max}(1-S_e)^{-1/\lambda}$	$P_{\max}$, λ: Physically based fitting parameters	First category
Lambda (L) (Wiltgen et al., 2003)	$S_w = a_L P_c^{-\lambda} + b_L$	λ: Physically based fitting parameter; b_L, a_L: Fitting parameters	First category
Van Genuchten (VG) (Van Genuchten, 1980)	$S_e = [1+(a_{VG}P_c)^{n_{VG}}]^{-m_{VG}}$	a_{VG}, n_{VG}: Physically based fitting parameters; $m_{VG} = 1-1/n_{VG}$ (fitting parameter)	Second category (Flexible, heterogeneous rocks)
Kosugi (K) (Kosugi, 1996)	$S_e = \frac{1}{2}\mathrm{erfc}\left(\frac{\ln P_c - \ln P_m}{\sqrt{2}w_K}\right)$	P_m, w_K: Physically based fitting parameters	Second category
Jing and Van Wunnik (JV) (Jing and Van Wunnik, 1998)	$P_c = P_c^0\left[\left(\frac{d_{JV}}{S_w - S_{wr}}\right)^{n_{JV}} + a_{JV}\right]$	P_c^0, d_{JV}, n_{JV}, a_{JV}: Fitting parameters; S_{wr}: Physically based fitting parameter	Second category
Johnson (J) (Johnson, 1987)	$\log(S_w) = A_J \log k + b_J P_c^{c_J}$	A_J, b_J, c_J: Fitting parameters; k: Pphysically based input parameter	Second category
Skelt and Harrison (SH) (Skelt and Harrison, 1995)	$S_w = 1-A_{SH}\exp\left[-\left(\frac{B_{SH}}{h+D_{SH}}\right)^{C_{SH}}\right]$	A_{SH}, B_{SH}, C_{SH}, D_{SH}: Fitting parameters; h: Physically based input parameter	Second category

Skelt and Harrison (1995) presented an empirical model to elucidate the link between water saturation and elevation above the free water level. The use of a logarithm in its correlation to represent this relationship is the model's strength since it provides a fitted curve shape that is similar to a capillary pressure curve (Behrenbruch et al., 2016). According to Lalanne and Rebelle, 2014, there are numerous analogies between the Skelt-Harris and Thomeer fit. A primary distinction between these two models is that the Skelt-Harrison (SH) model is suitable for experiments with low capillary pressures (centrifuges and porous plates), whereas T model has been developed to fit MICP experiments with capillary pressures above 10,000 psi. As a result, T model is a more general solution to P_c fitting than the SH one. The model is described by the following equation:

$$S_w = 1-A_{SH}\exp\left[-(\frac{B_{SH}}{h+D_{SH}})^{C_{SH}}\right] \quad (17)$$

where A_{SH}, B_{SH}, C_{SH}, and D_{SH} are fitting parameters and h is the height above free water level (m) which can be written in the term of pressure according to below:

$$h = \frac{P_c}{1000(\rho_{water}-\rho_{gas})g} \quad (18)$$

where ρ is the fluid density (kg/m^3).

Table 1 summarizes the capillary pressure models used in

this study, along with their parameter definitions.

2.2 Relative permeability models

Several empirical formulations are available for characterizing CO_2-brine relative permeability curves. These models are based on experimental observations, theoretical principles, and heuristic approaches. Each model comprises a set of parameters that are typically estimated by fitting experimental data (Honarpour et al., 1982; Moghadasi et al., 2015). Purcell (1949) introduced a method for determining relative permeability by deriving pore size distribution from mercury-injection capillary pressure curves. This method allows for the calculation of relative permeabilities in multiphase systems (Gates and Lietz, 1950; Li and Horne, 2006). The following equations can be used to determine relative permeability based on the effective saturation for both wetting and non-wetting phases:

$$\begin{aligned} k_{rw} &= S_e^{1+2/\lambda} \\ k_{rnw} &= 1 - S_e^{1+2/\lambda} \end{aligned} \tag{19}$$

The Corey model (Corey, 1954) is the most widely used since it is simple, requires few data points, and is simple to estimate due to the small number of parameters. This model is based on capillary pressure concepts and is generally considered to be accurate for consolidated porous media (Honarpour et al., 1982; Moghadasi et al., 2015). Consolidated media typically have well-defined pore structures and stable grain arrangements, which align well with the hypotheses of the Corey model. However, through appropriate tuning of its parameters, the model can also be applied to unconsolidated sands (Moghadasi et al., 2015). Unconsolidated sands, described by loose grain packing and higher porosity, require adjustments to λ and endpoint relative permeabilities to account for their unique flow behavior. Moreover, clay or other fine particles in unconsolidated media can further influence the relative permeability curves, as these materials can change pore connectivity and fluid flow paths. By including these factors in the parameter-tuning process, the Corey model can effectively capture the relative permeability behavior in both consolidated and unconsolidated porous media:

$$\begin{aligned} k_{rw} &= k_{rw}^{nw} S_e^{N_w} \\ k_{rnw} &= k_{rnw}^{w} (1 - S_e)^{N_{nw}} \end{aligned} \tag{20}$$

where k_{rw} and k_{rnw} are wetting and non-wetting phase relative permeabilities. k_{rw}^{nw} and k_{rnw}^{w} are the endpoints of relative permeability curves for the wetting and non-wetting phases, respectively. N_w and N_{nw} are fitting parameters that must be estimated since they determine the curvature of the relative permeability curves (Moghadasi et al., 2015).

Another model for representing the relationship between relative permeability and effective saturation is the Brooks Corey-Mualem (BCM) model (Brooks and Corey, 1966; Mualem, 1976):

$$\begin{aligned} k_{rw} &= \sqrt{S_e}\left[1 - (1 - S_w)^{A_{BCM}}\right]^2 \\ k_{rnw} &= \sqrt{1 - S_e}(1 - S_w^{A_{BCM}})^2 \end{aligned} \tag{21}$$

where $A_{BCM} = (1+\lambda)/\lambda$.

The Van Genuchten-Mualem (VGM) model (Mualem, 1976; Van Genuchten, 1980) describes the wetting phase relative permeability as follows:

$$k_{rw} = S_e^{a_{VGM}}\left[1 - (1 - S_e^{1/m_{VGM}})^{m_{VGM}}\right]^2 \tag{22}$$

where m_{VGM} and a_{VGM} are fitting parameters. They also presented the following equation for the relative permeability of the non-wetting phase:

$$k_{rnw} = S_{n,e}^{b_{VGM}}\left[1 - (1 - S_{n,e})^{1/m_{a,VGM}}\right]^{2m_{a,VGM}} \tag{23}$$

where b_{VGM} and $m_{a,VGM}$ are fitting parameters and $S_{n,e}$ is considered as effective non-wetting phase saturation, which is defined as follows:

$$S_{n,e} = 1 - S_e \tag{24}$$

The following exponential relationship was proposed by Chierici (1984) to determine the relative permeability of the wetting and non-wetting phases:

$$\begin{aligned} k_{rw} &= k_{rw}^{nw} \exp\left(-B_C S_e^{-M_C}\right) \\ k_{rnw} &= k_{rnw}^{w} \exp\left(-A_C S_e^{L_C}\right) \end{aligned} \tag{25}$$

where B_C, A_C, M_C, and L_C are the fitting parameters of the model that are estimated via the curve fit process. These parameters are not entirely unconstrained; they are subject to physical interpretations and constraints based on the underlying fluid flow behavior in porous media. In fact, parameters B_C and A_C control the curvature of the relative permeability curves near the endpoints (i.e., near residual saturations). They are related to the pore size distribution and the connectivity of the pore network, with higher values indicating more pronounced curvature due to heterogeneous pore structures. M_C and L_C influence the slope and shape of the relative permeability curves in the intermediate saturation range. They are associated with tortuosity and flow resistance within the porous medium, with larger values reflecting more complex flow paths. These parameters are also constrained during the fitting process to ensure that the resulting curves remain physically realistic. For example, the relative permeability values must lie between 0 and 1, and the curves must exhibit monotonic behavior (i.e., no oscillations or unrealistic inflections). Moreover, the parameters are often initialized based on prior knowledge of the rock and fluid properties, such as pore size distribution and wettability, to guide the optimization process.

According to these formulations (Eq. (25), experimental relative permeability curves are reasonably well-matched (Moghadasi et al., 2015). Compared to the Corey model and other polynomial approximations, the Chierici model provides better predictions at and near the initial and endpoints of the curves (Feigl, 2011). This improved performance is attributed to the model's ability to capture the nonlinear behavior of relative permeability in heterogeneous porous media. Due to its flexibility in representing both concave and convex relative permeability curves, the Chierici model is widely regarded as one of the best models for complex systems (Moghadasi et al., 2015). However, it is important to note that the model's

Table 2. Summary of relative permeability models used in this study, along with their parameter definitions.

Model	Formula	Declaration
Purcell (Purcell, 1949)	$k_{rw} = S_e^{1+2/\lambda}$ $k_{rnw} = 1 - S_e^{1+2/\lambda}$	S_e: Its wetting and non-wetting residual saturations can be physically based fitting parameters; λ: Physically based fitting parameter
(Corey, 1954)	$k_{rw} = k_{rw}^{nw} S_e^{N_w}$ $k_{rnw} = k_{rnw}^{w}(1 - S_e)^{N_{nw}}$	k_{rw}^{nw} and k_{rnw}^{w}: Physically based input parameters; N_w, N_{nw}: Partially physically based fitting parameter
Brooks Corey Mualem (BCM) (Mualem, 1976)	$k_{rw} = \sqrt{S_e}\left[1 - (1 - S_w)^{A_{BCM}}\right]^2$ $k_{rnw} = \sqrt{1 - S_e}(1 - S_w^{A_{BCM}})^2$	$A_{BCM} = 1 + 1/\lambda$: Partially physically based fitting parameter
Van Genuchten-Mualem (VGM) (Mualem, 1976)	$k_{rw} = (S_e)^{a_{VGM}}\left[1 - (1 - S_e^{1/m_{VGM}})^{m_{VGM}}\right]^2$ $k_{rnw} = (S_{n,e})^{b_{VGM}}\left[1 - (1 - S_{n,e})^{1/m_{a,VGM}}\right]^{2m_{a,VGM}}$	a_{VGM}, b_{VGM}: Fitting parameters; m_{VGM}, $m_{a,VGM}$: Physically based fitting parameter; $S_{n,e}$: Its wetting and non-wetting residual saturations can be physically based fitting parameters
Chierici (Chierici, 1984)	$k_{rw} = k_{rw}^{nw} \exp\left(-B_C S_e^{-M_C}\right)$ $k_{rnw} = k_{rnw}^{w} \exp\left(-A_C S_e^{L_C}\right)$	B_C, A_C, M_C, L_C: Partially physically based fitting parameters
L.E.T (Lomeland et al., 2005)	$k_{rw} = k_{rw}^{nw} \frac{S_e^{L_w}}{S_e^{L_w} + E_w(1 - S_e)^{T_w}}$ $k_{rnw} = k_{rnw}^{w} \frac{(1 - S_e)^{L_{nw}}}{(1 - S_e)^{L_{nw}} + E_{nw} S_e^{T_{nw}}}$	L_w, L_{nw}, E_w, E_{nw}, T_w, T_{nw}: Fitting parameters

accuracy depends on the quality of the experimental data and the careful application of physical constraints during the fitting process.

Another model that expresses the relationship between relative permeability and effective saturation is the L.E.T model (Lomeland et al., 2005):

$$k_{rw} = k_{rw}^{nw} \frac{S_e^{L_w}}{S_e^{L_w} + E_w(1 - S_e)^{T_w}}$$
$$k_{rnw} = k_{rnw}^{w} \frac{(1 - S_e)^{L_{nw}}}{(1 - S_e)^{L_{nw}} + E_{nw} S_e^{T_{nw}}} \quad (26)$$

where L_w, T_w, E_w, L_{nw}, E_{nw}, and T_{nw} are the fitting parameters. T (T_w, T_{nw}) and L (L_w, L_{nw}) drive the lower and upper portions of the relative permeability curve, respectively, while E represents the slope and elevation of the central part. Therefore, this model accurately reflects the variable behavior across a wide range of water saturation by including various segments of the relative permeability curve (Lomeland et al., 2005; Lomeland and Ebeltoft, 2013).

This section introduced some of the most widely used models, summarized in Table 2 along with their parameter definitions. Each model has a specific hypothesis but also has some limitations. Therefore, it is essential to select the most efficient model based on the properties and conditions.

2.3 Experimental data

Several methods exist for measuring capillary pressure, including MICP, porous plate, centrifuge, and dynamic capillary pressure techniques (Brown, 1951; Al-Bulushi et al., 2019). The literature indicates that experimental data for the CO_2-brine system is limited due to the high costs and time required (Bachu and Bennion, 2008; Bennion and Bachu, 2010). As a result, converting MICP data for use in CO_2-brine systems has become a common practice. However, while the conversion of MICP data using the Young-Laplace relation is widely employed to estimate capillary pressure, its accuracy has yet to be fully validated. Consequently, MICP results cannot reliably represent reservoir conditions (Pini et al., 2012). Therefore, this study focused on direct CO_2-brine data for capillary pressure and relative permeability experiments, excluding MICP data at this stage.

There are two common laboratory procedures for measuring relative permeability: Steady-state (SS) and unsteady-state (USS) methods. Relative permeability measurements made in laboratories using both SS and USS approaches are also microprocesses since only one measurement cannot accurately represent the entire reservoir (Ibrahim and , 2001). The steady-state method stands out as the most reliable technique among the developed methods for measuring relative permeability (Shen, 1988; Maini et al., 1990; Nazari Moghaddam and Jamiolahmady, 2019). However, they are intrinsically time-consuming since reaching equilibrium at each saturation level may take several hours or days. Their benefits encompass enhanced reliability and the ability to evaluate relative permeability across a broader spectrum of saturation levels. The Hassler approach, stationary phase, single-sample dynamic, Penn State, and modified Penn State are a few of the steady-state methods (Honarpour and Mahmood, 1988). Unsteady state approaches are the quickest ways to measure relative permeability in a laboratory setting. A typical implementation

Table 3. The statistical review of fluid and rock properties for samples used in capillary pressure experiments.

Property		Sandstone	Carbonate
ϕ (%)	min	3.50	19.03
	max	38.10	38.00
	avg	23.20	26.85
k (mD)	min	0.0007	13.600
	max	202,650	39,517
	avg	35,917	15,907
σ (mN/m)	min	22.30	28.10
	max	71.00	46.00
	avg	39.88	34.06
ρ_{brine} (gr/cm^3)	min	0.989	1.024
	max	1.123	1.050
	avg	1.031	1.033
ρ_{CO_2} (gr/cm^3)	min	0.002	0.001
	max	0.820	0.658
	avg	0.401	0.263

Notes: Such high values in the permeability and porosity of sandstone and carbonate formations are due to experiments carried out by Plug and Bruining (2007) on unconsolidated quartz sand and Wang and Tokunaga (2015) on limestone sand.

Table 4. The statistic review of fluid and rock properties for samples used in relative permeability experiments.

Property		Sandstone	Carbonate	Shale
ϕ (%)	min	0.26	7.90	3.90
	max	33.10	19.03	4.40
	avg	18.41	12.83	4.15
k (mD)	min	0.01	0.02	2.94E-06
	max	3,812	371.90	3.54E-04
	avg	332.03	87.79	1.45E-04
σ (mN/m)	min	19.80	28.10	19.80
	max	57.00	45.30	39.50
	avg	34.55	33.50	28.97
ρ_{brine} (gr/cm^3)	min	0.989	1.050[1]	/
	max	1.123	1.050	/
	avg	1.025	1.050	/
ρ_{CO_2} (gr/cm^3)	min	0.041	0.609	0.497
	max	0.856	0.811	0.824
	avg	0.577	0.695	0.671

Notes: [1]In the database, there was only one record.

involves injecting a driving fluid at a constant rate (or constant pressure) while continuously monitoring the effluent volume to move fluids in situ (Jones and Roszelle, 1978). All the available data for both capillary pressure and relative permeability are shown in the supplementary material file, and a statistical overview of them is presented in Tables 3 to 5.

The majority of experiments in literature have been conducted on sandstone samples. Additionally, there is significantly more data available on drainage than on imbibition with respect to relative permeability and capillary pressure. However, data on secondary drainage and imbibition remains insufficient. In sandstone formations, 78 capillary pressure experiments and 40 relative permeability experiments have been performed. In contrast, for carbonate formations, the number of experiments is much lower, with only 13 capillary pressure tests and 12 relative permeability tests.

2.4 Data processing

In data analysis, pre-processing is a crucial step. Thus, the collected data typically requires a series of processes before they can be analyzed and used. Failure to follow this procedure will result in erroneous analysis and outcomes. Several stages of pre-processing were applied to the collected data, including:

2.4.1 Data filtration

When working with lab data, filtration is often necessary due to factors such as human error, incorrect device calibration, and other inconsistencies. In a typical drainage experiment, an increase in capillary pressure should correspond to a decrease in saturation, while in a standard imbibition experiment, an increase in the saturation of the wetting phase should lead to a reduction in pressure. Any deviation from these expected trends is considered noise in this study, and efforts were made to minimize its impact. The remaining data points were treated as representative of a standard experiment. Data that showed significant deviation from the expected drainage or imbibition behavior were identified and excluded from the curve-fitting process. (Fig. 1). In fact, data points that did not follow these physical trends were excluded. Moreover, outlier detection calculations were applied to exclude data points falling outside the 95% confidence interval of the expected trend.

2.4.2 Closure correction

During the injection of the non-wetting phase, fluid may first enter larger pores (e.g., vugs) before reaching the main pore network of the sample (Abdollahian et al., 2019; Al-Bulushi et al., 2019). In other words, at the initial stage of drainage, the non-wetting phase may occupy pore spaces that are not part of the actual pore network. This phenomenon is referred to as the closure effect. Closure pressure is the pressure at which carbon dioxide enters the primary pore system of the sample. In industry, closure correction is commonly applied to MICP data due to the experimental setup. However, the data analyzed in this study pertains exclusively to the direct CO_2-brine system. Interestingly, some data exhibited behavior resembling the closure effect. To investigate these further, different models were fitted to the data both with and

Table 5. Number of experiments for capillary pressure and relative permeability in each process.

Saturation function	Process	Sandstone	Carbonate	Shale	Total
Capillary pressure	PD[1]	52	6	0	58
	PI[2]	18	6	0	24
	SD[3]	4	1	0	5
	SI[4]	4	0	0	4
Relative permeability	PD	24	9	3	36
	PI	16	3	3	22

Notes: [1]Primary drainage; [2]Primary imbibition; [3]Secondary drainage; [4]Secondary imbibition

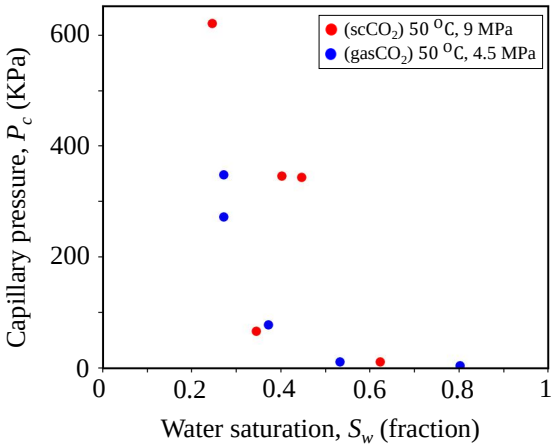

Fig. 1. Primary drainage capillary pressure on Indian limestone (El-Maghraby and Blunt, 2013). The blue symbols represent a reliable experiment, while the red symbols indicate an experiment that was excluded from analysis due to its irregular trend.

without applying closure correction. Fig. 2 shows the effect of the closure correction, representing a significant improvement in the accuracy of capillary pressure models, especially for those placed in the first category (Table 1). In experiments where closure effects are observed, it is crucial to extend laboratory data up to the inflection point (either the initial turning point or the first curvature). We determined the closure entry pressure by tracking it until its intersection with the pressure axis or until the water saturation reached 100% (Abdollahian et al., 2019).

2.4.3 X-axis reflection

Four of the experiments in the collected data are related to the forced imbibition process. Since the introduced models are incompatible with negative pressure, the data were transferred from negative pressure to positive using Eq. (27). During the transformation of data, we attempted to maintain the main trend of the chart:

$$y_{new} = (t_{\max} - t_{\min}) \frac{y - r_{\min}}{r_{\max} - r_{\min}} + t_{\min} \quad (27)$$

where $r_{\min}$ and $r_{\max}$ denote the minimum and maximum of measured data, respectively. $t_{\min}$ and $t_{\max}$ indicate the minimum and maximum of desired target scaling, respectively. The last two parameters were selected so that the data were symmetric with respect to the x-axis.

2.5 Optimization algorithm

Curve fitting, an essential component of this study, revolves around solving an optimization problem to determine the best-fitting line for a given set of observations. In this research, we employ the *curve fit* module within the SciPy library, specifically designed for nonlinear least squares curve fitting. The *curve fit* function requires several arguments, including input and output data, along with the designation of the mapping function. The objective is to utilize nonlinear least squares to optimize the coefficients of the mapping function, ensuring an optimal fit to the available input and output data.

The mapping function operates on input data examples and a set of arguments, which represent the coefficients or weight constants to be optimized through a nonlinear least squares optimization process. Also, the curve fit module has an optional initial guess for coefficients and a boundary condition, defining the range within which the optimal values will be determined. This module incorporates three optimization methods:

1) Trust Region Reflective Algorithm: Especially beneficial for tackling extensive sparse issues with established constraints.
2) Dogleg Algorithm with Rectangular Trust Regions: Suited for small scale problems with bounds.
3) Levenberg-Marquardt Algorithm: A robust algorithm for general purpose optimization. Does not accommodate bounds and sparse Jacobians. The most effective approach for minor unconstrained issues.

Given that constrained problems are prevalent in our scenarios, the Trust Region Reflective algorithm is selected as the preferred optimization method in most cases.

2.5.1 Assumptions

Curve fitting is the process of estimating model parameters by fitting them to valid experimental data. This process aimed to achieve the following goals:

1) Maximizing R^2 and minimizing RMSE.
2) Consideration of physical concepts.
3) The constants are always determined by the program unless the second rule is violated.

Boundary constraints are applied throughout the curve fitting process to ensure that irrational values are not obtained based on the physical concepts underlying each constant. Occasionally, it was necessary to force a fit if the physical concepts were violated or irrational values were specified for the parameters. During the curve force process, the following steps were considered:

1) Choosing an initial guess based on experimental data.

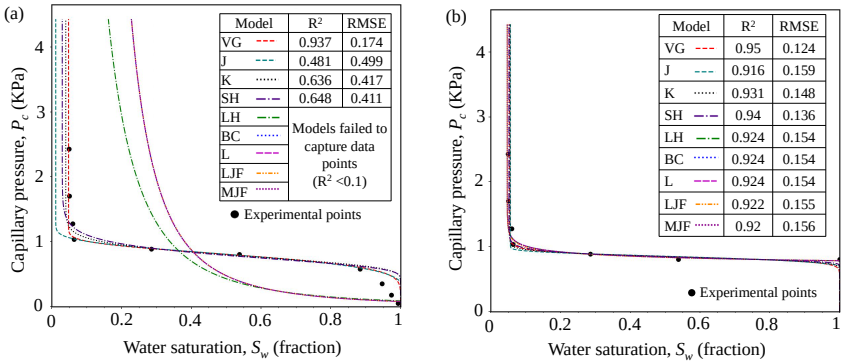

Fig. 2. The effect of closure correction on quartz sand pack (Tokunaga et al., 2013), as an example: (a) Before closure correction and (b) after closure correction.

2) Setting the constraints (step by step) on the values of physical parameters such as S_{wr}, P_e, etc.

If a model fails to fit through these two steps, then it has been ruled out of the analysis. The following two factors led to models being excluded from the analysis: (1) Negative R^2, which indicates that it is not a suitable model for this condition, (2) the model is out of trend data.

Several models are dependent on the rock and fluid properties of the sample (such as LJF, MJF, and SH models). As mentioned in Section 2.3, properties were calculated by correlation if they were not found in the literature.

3. Result and discussion

In this section, we compare the accuracy of the models discussed on both CO_2-brine capillary pressure and relative permeability data using the procedure mentioned in Section 2.

3.1 Capillary pressure models

Fig. 3 compares the accuracy of eleven capillary pressure models across different capillary pressure processes. In detail, Fig. 3(a) demonstrates the performance of the models introduced in Section 2.1 for PD process on Berea sandstone as an experiment representative of the general behavior of the data. The results indicate that all models effectively capture the experimental PD CO_2-brine capillary pressure, with the main difference being their accuracy in identifying the threshold pressure. Fig. 3(b) also compares the accuracy of the models for PI process. Based on the results from all experiments, we found that the BC, LH, and MJF models are less accurate than the others in this process. In contrast, the VG and K models accurately capture the experimental data. Finally, Figs. 3(c) and 3(d) represent the models' accuracy in two different experiments, respectively, from SD and SI processes. As with the PI, there is a significant discrepancy between the BC, LH, and MJF models and the experimental data. Therefore, let's focus on the physics behind these models and the reasons for their lower accuracy. Mathematically, these models (i.e., BC, LH, and MJF) exhibit power-law behavior and are physically capable of capturing the capillary pressure of samples with unimodal pore size distributions. Indeed, they are less suitable for cases with bi- or multimodal pore size distributions, which typically occur in the following scenarios:

1) when clays or other microporous minerals are present,
2) in vuggy carbonates,
3) in fractured rocks,
4) when two types of rocks are present for reservoir characterization.

For such complex cases, we found that flexible models, such as VG and K, better capture the CO_2-brine capillary pressure data.

Fig. 4 presents the models' performance based on the average RMSE and R^2 values for sandstone cases and carbonate rocks in different capillary pressure scenarios. For sandstone cases, the VG, SH, K, J, and JV models demonstrated the best performance, with R^2 values ranging from 0.967 to 0.98. In PI process, the VG and K models show superior results, with R^2 values between 0.996 and 0.997. Regarding SD, the VG and K models show the best accuracy, with average R^2 values of 0.989 for VG and 0.984 for K. Also, in SI, same as the PI and SD, titles for the most accurate models belong to the VG and K models, with VG slightly outperforming K. In carbonates, we observed similar results. Briefly, the VG, SH, K, J, and JV models more accurately captured the PD process. However, the VG and K models achieved the highest accuracy in the PI process, with R^2 values of 0.988 and 0.984, respectively.

We found that the studied capillary pressure models can be categorized into two groups:

1) **First Category**: BC, LH, LJF, MJF, L, and T models. These models exhibit power-law behavior and are suitable for more homogeneous rocks, particularly those with unimodal pore size distributions.
2) **Second Category**: VG, SH, K, J, and JV models. These models are mathematically flexible and can capture the capillary pressures of rocks with a broader range of heterogeneity.

Although the models are classified into two groups, their performance varies. For example, T model in the first group is relatively weak, as we found, due to its hyperbolic character. In the second category, some models (e.g., JV and J) also

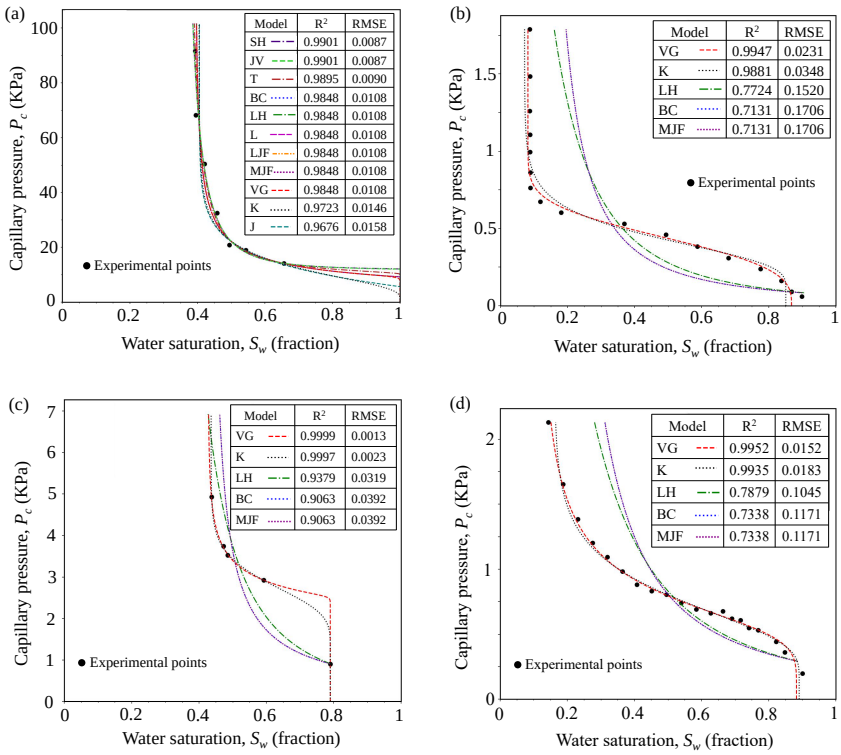

Fig. 3. The accuracy of the studied capillary pressure models across different capillary pressure processes. In all panels, data points represent experiments, and curves correspond to different models: (a) PDprocess-experiment 4 (Al-Menhali et al., 2015), (b) PI process. Supercritical CO_2 at 8.5 MPa-first cycle (Tokunaga et al., 2013), (c) SD process conducted on Bentheimer 3 rock sample (Abdoulghafour et al., 2020), and (d) SI process-experiment 13 (Plug and Bruining, 2007).

show lower accuracy than others. Within the first category, the LJF, MJF, and Lambda models exhibit similar accuracy to the BC model in all experiments. The BC model also shows results close to the LH models, particularly for the pore size distribution parameter, λ. According to Fig. 4, the capillary pressure models in the first category are highly dependent on closure correction, whereas the second category models are less dependent. The reason for this, as mentioned previously, is that models in the first category are limited to fitting a single curvature (power-law behavior), while models in the second category can handle multiple curvatures. Interestingly, it can be deduced that this feature in the second category improves the accuracy of detecting and adjusting the closure effect.

There are two other factors that improve the comparison and ranking of capillary pressure models: 1) the number of fitting parameters, and 2) the nature of the fitting parameters (whether they are physically based or empirical). Table 1 summarizes the capillary pressure models used in this study, along with their parameter definitions, highlighting which parameters are physically based and which are empirical fitting parameters, as well as the assigned categories for each model. Considering both the number of fitting parameters in Table 1 and Fig. 4, we can find that the K model shows superior results, among the capillary pressure models with high accuracy indices (Fig. 4). With only two fitting parameters (P_m and w_K), it achieves high accuracy while minimizing the risk of overfitting. In contrast, models like JV and SH models, which have four fitting parameters, may offer more flexibility but are more prone to overfitting, especially in cases with limited experimental data. Moreover, although more fitting parameters may capture data well, their uncertainty and practical application for new data are often questionable.

When considering the number of fitting parameters, along with the physical interpretation of the models, we find that the K model's superiority is further reinforced by its physical basis. The K model assumes a lognormal distribution of pore sizes, which is physically meaningful for many natural porous media. The parameters P_m (median pore radius) and w_K (standard deviation of log-transformed pore size) have physical interpretations, making the model more robust for practical applications.

3.2 Relative permeability models

Figs. 5 and 6 compare the performance of relative permeability models for both brine and CO_2 phases during drainage and imbibition processes. Fig. 5 indicates that, except for the BCM model, most models yield acceptable results for Tuscaloosa sandstone in primary drainage. The Chierici, LET, VGM, and Corey models, in particular, show high R^2 values and accurately capture the relative permeability data for both phases. Fig. 6 also presents the imbibition process on Chaunoy sandstone, where the models' accuracy is comparable to that observed in the drainage process.

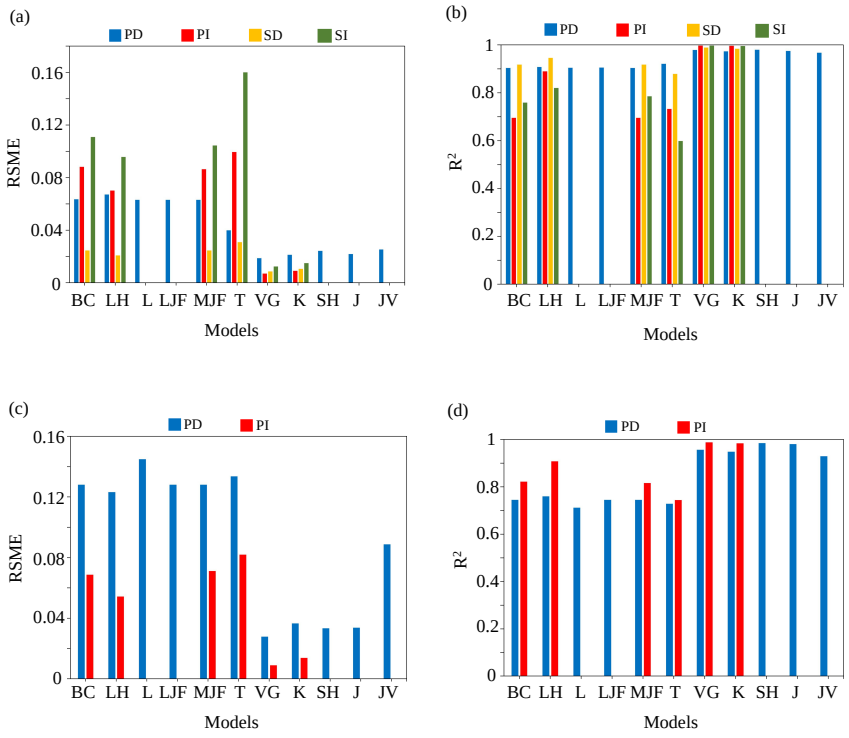

Fig. 4. Comparison of the accuracy of studied capillary pressure models applied to CO_2-brine data from various formations in different capillary pressure processes for all available data. (a) and (b) illustrate the accuracy of the models based on R^2 and RMSE values in sandstone formations, respectively. (c) and (d) also compare R^2 and RMSE values corresponding to each model in carbonate rocks.

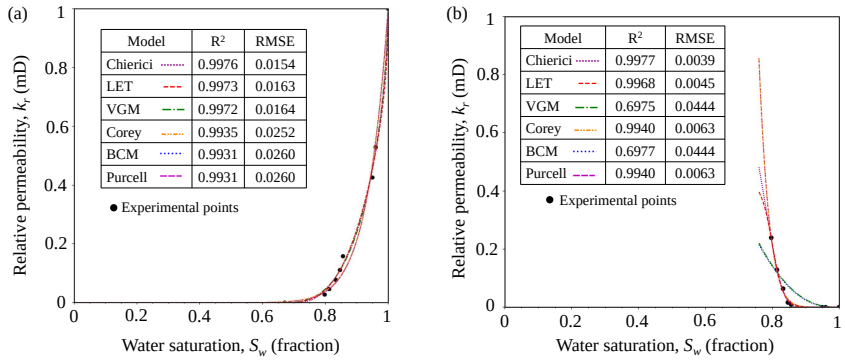

Fig. 5. Comparison of the studied models in primary drainage CO_2-brine relative permeability: (a) PD process for brine phase-Tuscaloosa sandstone (Bakhshian and Hosseini, 2019) and (b) PD process for CO_2 phase-Tuscaloosa sandstone (Bakhshian and Hosseini, 2019).

Figs. 7 and 8 present the accuracy of the models based on the collected CO_2-brine relative permeability data for sandstone, carbonate, and shale cases, considering both PD and PI processes. According to Fig. 7, the VGM, Chierici, and L.E.T models showed the best performance for the PD process in brine phase across sandstone, carbonate, and shale formations. In detail, for sandstone, the L.E.T, VGM, and Chierici models had the highest average R^2 values of 0.9929, 0.9892, and 0.9855, respectively. BCM, Purcell, and Corey were less accurate, with average R^2 values of 0.8949, 0.9567, and 0.9594. In carbonate formations, all six models achieved average R^2 values above 0.995. In shale formations, all models performed well except BCM, which had a low average R^2 of 0.5256 (note that only two experiments were available for shale in the PD process). For CO_2 phase in the PD process (Fig. 8), the L.E.T, Chierici, and Corey models performed best in sandstone, with average R^2 values of 0.9907, 0.9734, and 0.9690, respectively. VGM, Purcell, and BCM had lower R^2 values of 0.8969, 0.7909, and 0.7634. In carbonate formations, L.E.T, Corey, and Chierici had superior results, with average

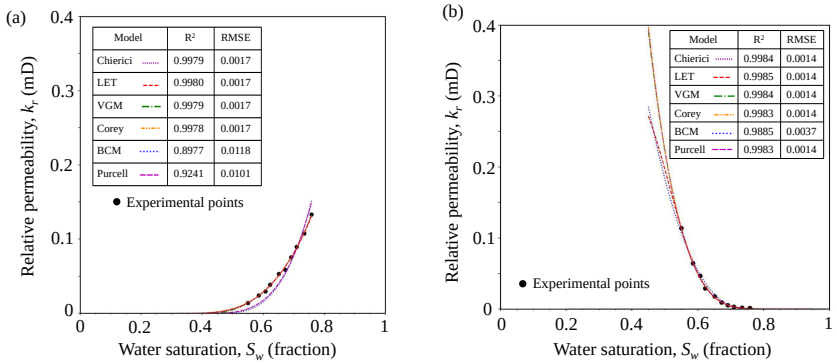

Fig. 6. Comparison of the studied models in primary imbibition CO_2-brine relative permeability: (a) PI process for brine phase-Chaunoy Sandstone (Manceau et al., 2015) and (b) PI process for CO_2 phase-Chaunoy Sandstone (Manceau et al., 2015).

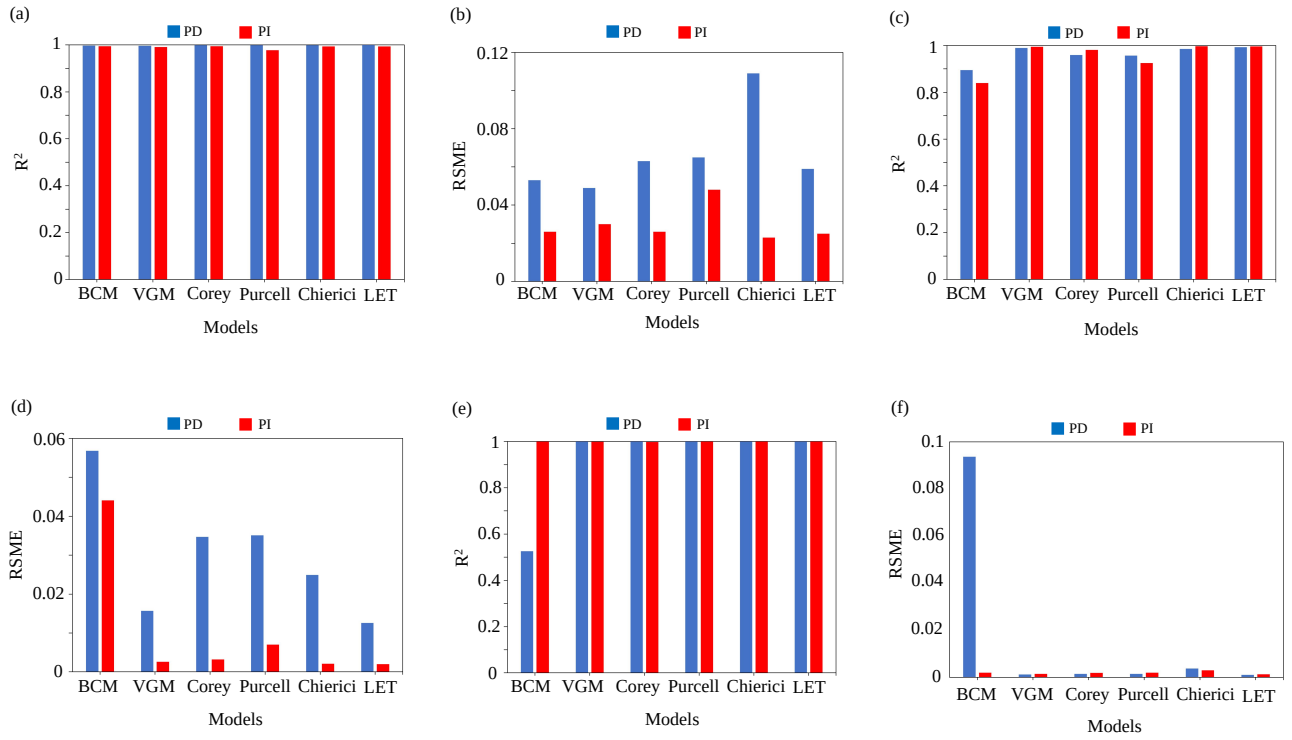

Fig. 7. Comparison of the accuracy of studied relative permeability models applied to all available data for the brine phase in both drainage and imbibition processes. (a) and (b) present the accuracy of the models based on R^2 and RMSE values in carbonate formations, respectively. (c) and (d) show the same metrics in sandstone formations, and (e) and (f) indicate the metrics for shale data.

R^2 values of 0.9991, 0.9986, and 0.9980, respectively, while VGM, Purcell, and BCM performed less well. In shale formations, L.E.T, Chierici, and Corey also showed the best results.

In the PI process, for brine phase, the VGM, Chierici, and L.E.T models showed the best results in sandstone cases, with average R^2 values of 0.9944, 0.9972, and 0.9965, respectively. Corey's model, with an average R^2 of 0.9813, performed well but was less accurate than the top three models. The Purcell and BCM models, with mean R^2 values of 0.8398 and 0.925, were less accurate. In carbonate formations, all models performed well, with average R^2 values above 0.99, except for Purcell, which had a R^2 of 0.9772. In shale formations, all six models showed high accuracy. For CO_2 phase in the PI process, the L.E.T, Corey, and Chierici models again performed best, with average R^2 values of 0.9938, 0.9890, and 0.9933, respectively. VGM also performed well with an average R^2 of 0.9759, while Purcell and BCM showed less accurate results. In shale formations, all models had also average R^2 values above 0.99.

Considering the fitting results based on R^2 and RMSE metrics across various scenarios, we can find that for the brine phase, the most suitable models are L.E.T., Chierici,

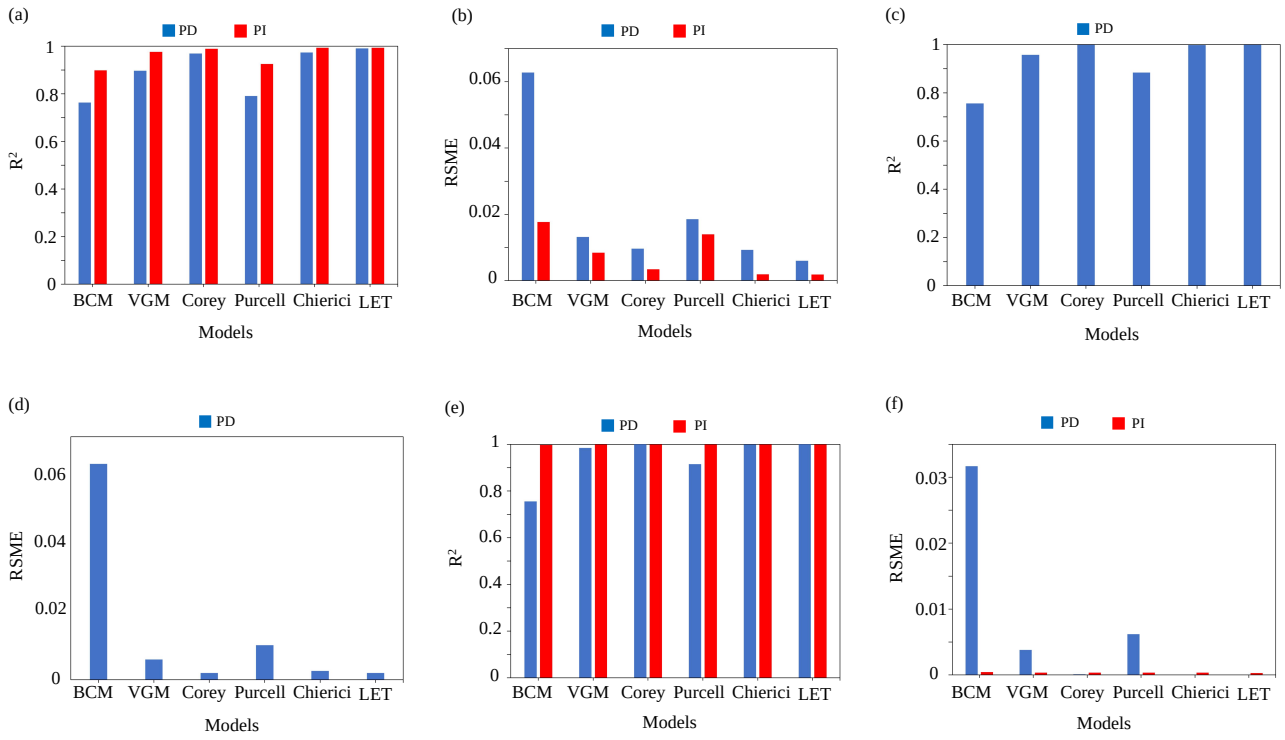

Fig. 8. Comparison of the accuracy of studied relative permeability models applied to all available data for the CO_2 phase in both drainage and imbibition processes. (a) and (b) present the accuracy of the models based on R^2 and RMSE values in sandstone formations, respectively. (c) and (d) show the same metrics in carbonate formations, and (e) and (f) indicate the metrics for shale data.

VGM, and Corey, in that order. For the CO_2 phase, the L.E.T., Chierici, Corey, and VGM models were found to be the most reliable. In drainage cases, the L.E.T., Chierici, and Corey models exhibited superior performance. Similarly, for the PI process, the L.E.T., Chierici, Corey, and VGM models provided a more accurate representation of relative permeability data. When examining performance across different formations, the L.E.T., Chierici, Corey, and VGM models consistently delivered better results for sandstone formations. For carbonate formations, the L.E.T., Chierici, VGM, and Corey models also outperformed others. In the case of shale formations, all models performed comparably well. In this context, it is important to note that the success of the models also depended on the pore distribution and mean pore size of the formations. Thus, the sandstone formations, with a rather homogeneous pore structure, are more adapted to simpler models such as Corey and VGM, which need fewer fitting parameters and are therefore more robust for practical applications. In contrast, the carbonate and shale formations generally have more complicated pore structures, like vugs, fractures, or microporosity, which demand more flexible models such as L.E.T. and Chierici for a better description of their heterogeneity.

Building on these findings, we can further assess the accuracy of models in capturing CO_2-brine relative permeability data. The L.E.T., Chierici, Corey, and VGM models demonstrated strong and nearly identical performance. However, as observed in the results for capillary pressure models, further comparison of relative permeability models can be enhanced by considering two key factors: the number of fitting parameters and the nature of those parameters (i.e., whether they are physically based or empirical). In this context, the L.E.T. model requires more fitting parameters than the other models. Specifically, the L.E.T. model includes six parameters (L_w, E_w, T_w, L_{nw}, E_{nw}, T_{nw}), while the Chierici model uses four (B_C, A_C, M_C, and L_C). More fitting parameters provide additional flexibility, enabling a model to capture complex relative permeability curves with high accuracy, but they also increase susceptibility to overfitting, particularly when experimental data are limited. In contrast, simpler models like Corey, with fewer fitting parameters, offer greater robustness and practicality, especially in formations with more uniform pore structures. For heterogeneous cases or complex relative permeability data points, between the Chierici and VGM models, the VGM model, derived from its capillary pressure model, presents more physically based fitting parameters, which can be regarded as the better model. In conclusion, among the studied models, the Corey model, with the fewest fitting parameters, offers simplicity and practicality, while the VGM model, with more physically based parameters, provides greater adaptability for complex formations and data sets.

4. Conclusions

We evaluated the accuracy of eleven capillary pressure models and six relative permeability models for the CO_2-brine system, considering various rock types (such as carbonate and sandstone) and processes (such as drainage and imbibition). The findings of this study, separately for capillary pressure and relative permeability data, are as follows:

4.1 Capillary pressure

1) The capillary pressure models studied can be categorized into two classes. The first class includes the BC, LJF, MJF, LH, L, and T models. These models exhibit power-law behavior and are more suitable for homogeneous rock samples with unimodal pore size distribution. The second class comprises VG, SH, JV, K, and J models. These models are mathematically flexible and can capture more heterogeneous cases, such as rocks with bi- or tri-modal pore size distributions. However, despite the categorization, models within each class sometimes exhibited varying accuracy.
2) Using models from the second category improves the detection and correction of closure effects in capillary pressure data.
3) This study suggests that the VG and K models better capture capillary pressure curves across all cycles and rock types in the CO_2-brine system. However, since the K model includes meaningful physical parameters, it is recommended for use in studies and simulations.

4.2 Relative permeabilitytle

1) The L.E.T., Chierici, VGM, and Corey models demonstrate strong, nearly identical performance for both PD and PI processes across all formation types and phases (brine and CO_2). Among these, the Corey model, with the fewest fitting parameters, offers simplicity and practicality, while the VGM model, with more physically based parameters, provides greater adaptability for complex formations.
2) Among the studied relative permeability models, the VGM model outperformed the others in the brine phase, while the Corey model performed best in the CO_2 phase.

Conflict of interest

The authors declare no competing interest.

References

Abdollahian, A., Tadayoni, M., Junin, R. B. A new approach to reduce uncertainty in reservoir characterization using saturation height modeling, Mesaverde tight gas sandstones, western US basins. Journal of Petroleum Exploration and Production Technology, 2019, 9(3): 1953-1961.

Abdoulghafour, H., Sarmadivaleh, M., Hauge, L. P., et al. Capillary pressure characteristics of CO_2-brine-sandstone systems. International Journal of Greenhouse Gas Control, 2020, 94: 102876.

Akbarabadi, M., Piri, M. Relative permeability hysteresis and capillary trapping characteristics of supercritical CO_2/brine systems: An experimental study at reservoir conditions. Advances in Water Resources, 2013, 52: 190-206.

Alizadeh, A. H., Piri, M. Three-phase flow in porous media: A review of experimental studies on relative permeability. Reviews of Geophysics, 2014, 52(3): 468-521.

Al-Bulushi, N., King, P. R., Blunt, M. J., et al. Development of artificial neural network models for predicting water saturation and fluid distribution. Journal of Petroleum Science and Engineering, 2009, 68(3-4): 197-208.

Al-Bulushi, N., Kraishan, G., Hursan, G. Capillary pressure corrections, quality control and curve fitting workflow. Paper IPTC 19514 Presented at the International Petroleum Technology Conference, Beijing, China, 26-28 March, 2019.

Al-Menhali, A., Niu, B., Krevor, S. Capillarity and wetting of carbon dioxide and brine during drainage in Berea sandstone at reservoir conditions. Water Resources Research, 2015, 51(10): 7895-7914.

Al Waili, I. H. Developing generalised capillary pressure curves and saturation height function for Shuaiba carbonate reservoirs in field A. Paper SPE 136191 Presented at the SPE Annual Technical Conference and Exhibition, New Orleans, Louisiana, 4-7 October, 2009.

Bachu, S., Bennion, B. Effects of in-situ conditions on relative permeability characteristics of CO_2-brine systems. Environmental Geology, 54(8): 1707-1722, 2008.

Bakhshian, S., Hosseini, S. A. Pore-scale analysis of supercritical CO_2-brine immiscible displacement under fractional-wettability conditions. Advances in Water Resources, 2019, 126: 96-107.

Bakhshian, S., Hosseini, S. A., Lake, L. W. CO_2-brine relative permeability and capillary pressure of Tuscaloosa sandstone: Effect of anisotropy. Advances in Water Resources, 2020, 135: 103464.

Behrenbruch, P., Huu, M. T., Hoang, T. G., et al. Modelling of drainage capillary pressure: A comparative study of various analytical capillary pressure formulations in matching laboratory results. Paper SPE 182469 Presented at the SPE Asia Pacific Oil & Gas Conference and Exhibition, Perth, Australia, 25-27 October, 2016.

Bennion, D. B., Bachu, S. Dependence on temperature, pressure, and salinity of the IFT and relative permeability displacement characteristics of CO_2 injected in deep saline aquifers. Paper SPE 102138 Presented at the SPE Annual Technical Conference and Exhibition, San Antonio, Texas, USA, 24-27 September, 2006.

Bennion, D. B., Bachu, S. Correlations for the interfacial tension between supercritical phase CO_2 and equilibrium brines at in-situ conditions. Paper SPE 114479 Presented at the SPE Annual Technical Conference and Exhibition, Denver, Colorado, USA, 21-24 September, 2008a.

Bennion, D. B., Bachu, S. Drainage and imbibition relative permeability relationships for supercritical CO_2 /brine and H2S /brine systems in intergranular sandstone, carbonate, shale, and anhydrite rocks. SPE Reservoir Evaluation & Engineering, 2008b, 11(3): 487-496.

Bennion, D. B., Bachu, S. Drainage and imbibition CO_2/brine relative permeability curves at reservoir conditions for carbonate formations. Paper SPE 134028 Presented at the SPE Annual Technical Conference and Exhibition, Florence, Italy, 19-22 September, 2010.

Berg, S., Oedai, S., Ott, H. Displacement and mass transfer between saturated and unsaturated CO_2-brine systems in sandstone. International Journal of Greenhouse Gas Control, 2013, 12: 478-492.

Brooks, R. H., & Corey, A. T. Properties of porous media affecting fluid flow. Journal of the Irrigation and Drainage Division, 1966, 92(2): 61-88.

Brown, H. W. Capillary pressure investigations. Journal of Petroleum Technology, 1951, 3(3): 67-74.

Chierici, G. L. Novel relations for drainage and imbibition relative permeabilities. Society of Petroleum Engineers Journal, 24(3): 275-276, 1984.

Choi, J. W., Nicot, J. P., Hosseini, S. A., et al. CO_2 recycling accounting and EOR operation scheduling to assist in storage capacity assessment at a U.S. Gulf Coast depleted reservoir. International Journal of Greenhouse Gas Control, 2013, 18: 474-484.

Christoffersen, K. R., Whitson, C. H. Gas/oil capillary pressure of chalk at elevated pressures. SPE Formation Evaluation, 1995, 10(3): 153-159.

Corey, A. T. The interrelation between gas and oil relative permeabilities. Producers Monthly, 1954, 19: 38-41.

Dai, Z., Zhang, Y., Bielicki, J., et al. Heterogeneity-assisted carbon dioxide storage in marine sediments. Applied Energy, 2018, 225: 876-883.

El-Maghraby, R. M., Blunt, M. J. Residual CO_2 trapping in Indiana limestone. Environmental Science & Technology, 47(1): 227-233, 2013.

Falkowski, P., Scholes, R. J., Boyle, E. E. A., et al. The global carbon cycle: A test of our knowledge of Earth as a system. Science, 2000, 290(5490): 291-296.

Faramarzi-Palangar, M., Mirzaei-Paiaman, A. Identifying two-phase flow rock types in CO_2-brine systems using TEM-function. Journal of Petroleum Science and Engineering, 2021, 205: 108818.

Faramarzi-Palangar, M., Mirzaei-Paiaman, A. Investigating dynamic rock quality in two-phase flow systems using TEM-function: A comparative study of different rock typing indices. Petroleum Research, 2021, 6(1): 16-25.

Faramarzi-Palangar, M., Sedaee, B., Niri, M. E. A further investigation on the application of critical pore size as an approach for reservoir rock typing. Journal of Energy Resources Technology, 2021a, 143(11): 112901.

Faramarzi-Palangar, M., Mirzaei-Paiaman, A., Ghoreishi, S. A., et al. Wettability of carbonate reservoir rocks: A comparative analysis. Applied Sciences, 2021b, 12(1): 131.

Feigl, A. Treatment of relative permeabilities for application in hydrocarbon reservoir simulation model. Nafta, 2011, 62(7-8): 233-243.

Gao, H., Yu, B., Duan, Y., et al. Fractal analysis of dimensionless capillary pressure function. International Journal of Heat and Mass Transfer, 2014, 69: 26-33.

Gates, J. I., Lietz, W. T. Relative permeabilities of California cores by the capillary-pressure method. Paper Presented at the Spring Meeting of the Pacific Coast District, Division of Production, Los Angeles, California, May, 1950.

Gdanski, R., Fulton, D., Shen, C. Fracture-face-skin evolution during cleanup. SPE Production & Operations, 2009, 24(1): 22-34.

Gershenzon, N. I., Ritzi Jr, R. W., Dominic, D. F., et al. Comparison of CO_2 trapping in highly heterogeneous reservoirs with Brooks-Corey and Van Genuchten type capillary pressure curves. Advances in Water Resources, 2016, 96: 225-236.

Goda, H. S., Behrenbruch, P. A universal formulation for the prediction of capillary pressure. Paper SPE 147078 Presented at the SPE Annual Technical Conference and Exhibition, Denver, Colorado, USA, 30 October-2 November, 2011.

Greder, H. N., Gallato, V., Cordelier, P., et al. Forty comparisons of mercury injection data with oil/water capillary pressure measurements by the porous plate technique. Paper SCA-9710 Presented at the Society of Core Analysis Symposium, Calgary, Alberta, Canada, 1997.

Hashemi, S. M. H., Monfaredi, K., Sedaee, B. An inclusive consistency check procedure for quality control methods of the black oil laboratory data. Journal of Petroleum Exploration and Production Technology, 2020, 10: 2153-2173.

Honarpour, M., Koederitz, L. F., Harvey, A. H. Empirical equations for estimating two-phase relative permeability in consolidated rock. Journal of Petroleum Technology, 1982, 34(12): 2905-2908.

Honarpour, M., Mahmood, S. M. Relative-permeability measurements: An overview. Journal of Petroleum Technology, 1988, 40(8): 963-966.

Hopmans, J. W., Grismer, M. E., Chen, J., et al. Parameter estimation of two-fluid capillary pressure saturation and permeability functions. Cincinnati, National Risk Management Research Laboratory, Office of Research and Development, USEPA, 1998.

Ibrahim, M. N., Koederitz, L. F. Two-phase steady-state and unsteady-state relative permeability prediction models. Paper SPE 68065 Presented at the SPE Middle East Oil Show, Manama, Bahrain, 17-20 March, 2001.

Iglauer, S., Pentland, C. H., Busch, A. CO_2 wettability of seal and reservoir rocks and the implications for carbon geo-sequestration. Water Resources Research, 2015, 51(1): 729-774.

Imbus, S. W., Orr, F. M., Kuuskraa, V. A., et al. Critical issues in CO_2 capture and storage: Findings of the SPE advanced technology workshop (ATW) on carbon sequestration. Paper SPE 102968 Presented at the SPE Annual Technical Conference and Exhibition, San Anto-

nio, Texas, USA, 24-27 September, 2006.

Ioannidis, M. A., Chatzis, I. Network modelling of pore structure and transport properties of porous media. Chemical Engineering Science, 1993, 48(5): 951-972.

Jia, W., McPherson, B., Pan, F., et al. Impact of three-phase relative permeability and hysteresis models on forecasts of storage associated with CO_2-EOR. Water Resources Research, 2018, 54(2): 1109-1126

Jing, X. D., Van Wunnik, J. N. M. A capillary pressure function for interpretation of core-scale displacement experiments. Paper SCA-9807 Presented at the Society of Core Analysts Symposium, the Hague, Netherlands, 14-16 September, 1998.

Johnson, A. Permeability averaged capillary data: A supplement to log analysis in field studies. Paper SPWLA-1987-EE Presented at the SPWLA 28th Annual Logging Symposium, London, England, 29 June-2 July, 1987.

Jones, S. C., Roszelle, W. O. Graphical techniques for determining relative permeability from displacement experiments. Journal of Petroleum Technology, 1978, 30(5): 807-817.

Kosugi, K. Lognormal distribution model for unsaturated soil hydraulic properties. Water Resources Research, 1996, 32(9): 2697-2703.

Lalanne, B., Rebelle, M. A review of alternative methods to classify rock-types from capillary pressure measurements. Paper cp-395-00124 Presented at the International Petroleum Technology Conference, Kuala Lumpur, Malaysia, 10-12 December, 2014.

Leverett, M. C., Lewis, W. B. Steady flow of gas-oil-water mixtures through unconsolidated sands. Transactions of the AIME, 1941, 142(1): 107-116.

Leverett, M. C. Capillary behavior in porous solids. Transactions of the AIME, 1941, 142(1): 152-169.

Li, B., Tchelepi, H. A., Benson, S. M. Influence of capillary-pressure models on CO_2 solubility trapping. Advances in Water Resources, 2013, 62: 488-498.

Li, K., Horne, R. N. An experimental and analytical study of steam/water capillary pressure. SPE Reservoir Evaluation & Engineering, 2001, 4(6): 477-482.

Li, K., Horne, R. N. Comparison of methods to calculate relative permeability from capillary pressure in consolidated water-wet porous media. Water Resources Research, 2006, 42(6): W06405.

Li, K., Horne, R. N. Fractal characterization of the Geysers rock. Paper Presented at the Geothermal Resources Council Annual Meeting, Morelia, Mexico, 12-15 October, 2003.

Li, K. Generalized capillary pressure and relative permeability model inferred from fractal characterization of porous media. Paper SPE 89874 Presented at the SPE Annual Technical Conference and Exhibition, Houston, Texas, 26-29 September, 2004.

Li, K. More general capillary pressure and relative permeability models from fractal geometry. Journal of Contaminant Hydrology, 2010, 111(1-4): 13-24.

Liu, R., Liu, H., Li, X., et al. Calculation of oil and water relative permeability for extra low permeability reservoir. Paper SPE 131388 Presented at the International Oil and Gas Conference and Exhibition in China, Beijing, 8-10 June, 2010.

Lomeland, F., Ebeltoft, E. Versatile three-phase correlations for relative permeability and capillary pressure. Paper SCA2013-034 Presented at the International Symposium of the Society of Core Analysts, Napa Valley, California, USA, 16-19 September, 2013.

Lomeland, F., Ebeltoft, E., Thomas, W. H. A new versatile relative permeability correlation. Paper SCA-2005-112 Presented at the International Symposium of the Society of Core Analysts, Toronto, Canada, 21-25 August, 2005.

Maini, B., Coskuner, G., Jha, K. A comparison of steady-state and unsteady-state relative permeabilities of viscous oil and water in Ottawa sand. Journal of Canadian Petroleum Technology, 1990, 29(2): PETSOC-90-02-02.

Manceau, J. C., Ma, J., Li, R., et al. Two-phase flow properties of a sandstone rock for the CO_2/water system: Core-flooding experiments, and focus on impacts of mineralogical changes. Water Resources Research, 2015, 51(4): 2885-2900.

Ma, S., Morrow, N. R. Relationships between porosity and permeability for porous rocks. Paper SCA-9610 Presented at the International Symposium of the Society of Core Analysts, Montpellier, France, 8-10 September, 1996.

Mirzaei-Paiaman, A., Faramarzi-Palangar, M., Djezzar, S., et al. A new approach to measure wettability by relative permeability measurements. Journal of Petroleum Science and Engineering, 2022, 208: 109191.

Moghadasi, L., Guadagnini, A., Inzoli, F., et al. Interpretation of two-phase relative permeability curves through multiple formulations and model quality criteria. Journal of Petroleum Science and Engineering, 2015, 135: 738-749.

Mualem, Y. A new model for predicting the hydraulic conductivity of unsaturated porous media. Water Resources Research, 1976, 12(3): 513-522.

Nasr, N. H. Integrating core and log data by using different saturation height functions (SHF). IRC, 2015.

Nazari Moghaddam, R., Jamiolahmady, M. Steady-state relative permeability measurements of tight and shale rocks considering capillary end effect. Transport in Porous Media, 2019, 128: 75-96.

Newsham, K. E., Rushing, J. A., Lasswell, P. M., et al. A comparative study of laboratory techniques for measuring capillary pressures in tight gas sands. Paper SPE 89866 Presented at the SPE Annual Technical Conference and Exhibition, Houston, Texas, 26-29 September, 2004.

Oostrom, M., White, M. D., Porse, S. L., et al. Comparison of relative permeability-saturation-capillary pressure models for simulation of reservoir CO_2 injection. International Journal of Greenhouse Gas Control, 2016, 45: 70-85.

Pentland, C. H., El-Maghraby, R., Iglauer, S., et al. Measurements of the capillary trapping of super-critical carbon dioxide in Berea sandstone. Geophysical Research Letters, 2011, 38(6): L06401.

Pini, R., Krevor, S. C. M., Benson, S. M. Capillary pressure and heterogeneity for the CO_2/water system in sand-

stone rocks at reservoir conditions. Advances in Water Resources, 2012, 38: 48-59.

Pini, R., Krevor, S., Krause, M., et al. Capillary heterogeneity in sandstone rocks during CO_2/water core-flooding experiments. Energy Procedia, 2013, 37: 5473-5479.

Plug, W. J., Bruining, J. Capillary pressure for the sand-CO_2-water system under various pressure conditions. Application to CO_2 sequestration. Advances in Water Resources, 2007, 30(11): 2339-2353.

Purcell, W. R. Capillary pressures: Their measurement using mercury and the calculation of permeability therefrom. Journal of Petroleum Technology, 1949, 1(2): 39-48.

Raza, A., Gholami, R., Rezaee, R., et al. Significant aspects of carbon capture and storage-a review. Petroleum, 2019, 5(4): 335-340.

Ren, W., Li, G., Tian, S., et al. Comparison of capillary pressure-saturation models for gas-water systems in shale gas reservoirs. Paper SPE 182461 Presented at the SPE Asia Pacific Oil & Gas Conference and Exhibition, Perth, Australia, 25-27 October, 2016.

Safari, H., Faramarzi-Palangar, M., Hashemi, S. M. H., et al. A new approach to 3D saturation height modeling by coupling a capillary pressure model with pore throat size distribution. Natural Resources Research, 2022, 31(2): 1045-1059.

Sarwaruddin, M., Skauge, A., Torsaeter, O. Modeling of capillary pressure for heterogeneous reservoirs by a modified J-Function. Paper SCA-2001-35 Presented at the Society of Core Analysts Symposium, Edinburgh, Scotland, 16-19 September, 2001.

Shen, J. S. Automated steady state relative permeability measurement system. US4773254, 1988.

Shi, S., Belhaj, H., Bera, A. Capillary pressure and relative permeability correlations for transition zones of carbonate reservoirs. Journal of Petroleum Exploration and Production Technology, 2018, 8(3): 767-784.

Silin, D., Tomutsa, L., Benson, S. M., et al. Microtomography and pore-scale modeling of two-phase fluid distribution. Transport in Porous Media, 2011, 86: 495-515.

Skelt, C., Harrison, B. An integrated approach to saturation height analysis. Paper SPWLA-1995-NNN Presented at the SPWLA 36th Annual Logging Symposium, Paris, France, 26-29 June, 1995.

Thomeer, J. H. M. Introduction of a pore geometrical factor defined by the capillary pressure curve. Journal of Petroleum Technology, 1960, 12(3): 73-77.

Tokunaga, T. K., Wan, J., Jung, J. W., et al. Capillary pressure and saturation relations for supercritical CO_2 and brine in sand: High-pressure $P_c(S_w)$ controller/meter measurements and capillary scaling predictions. Water Resources Research, 2013, 49(8): 4566-4579.

Tsakiroglou, C. D., Theodoropoulou, M. A., Karoutsos, V. Nonequilibrium capillary pressure and relative permeability curves of porous media. AIChE Journal, 2003, 49(10): 2472-2486.

Van Genuchten, M. Th. A closed-form equation for predicting the hydraulic conductivity of unsaturated soils. Soil Science Society of America Journal, 1980, 44(5): 892-898.

Wang, S., Tokunaga, T. K. Capillary pressure-saturation relations for supercritical CO_2 and brine in limestone/-dolomite sands: Implications for geologic carbon sequestration in carbonate reservoirs. Environmental Science & Technology, 2015, 49(12): 7208-7217.

Wang, X., Alvarado, V., Swoboda-Colberg, N., et al. Reactivity of dolomite in water-saturated supercritical carbon dioxide: Significance for carbon capture and storage and for enhanced oil and gas recovery. Energy Conversion and Management, 2013, 65: 564-573.

Wiltgen, N. A., Le Calvez, J., Owen, K. Methods of saturation modeling using capillary pressure averaging and pseudos. Paper SPWLA-2003-W Presented at the SPWLA 44th Annual Logging Symposium, Galveston, Texas, 22-25 June, 2003.

Sun, X., Mohanty, K. K. Estimation of flow functions during drainage using genetic algorithm. Paper presented at the SPE Annual Technical Conference and Exhibition, Denver, Colorado, 5-8 October, 2003.

Xu, W., Luo, P., Sun, L., et al. A prediction model of the capillary pressure J-function. PLoS ONE, 2016, 11(9): e0162123.

Yu, P., Archer, R. A fractal gas-water relative permeability model in geothermal reservoirs, in Proceedings, 44th Workshop on Geothermal Reservoir Engineering, Stanford University, Stanford, California, pp. 1-13, 2019.

Zhang, Y., Yang, D. Simultaneous estimation of relative permeability and capillary pressure for tight formations using ensemble-based history matching method. Computers & Fluids, 2013, 71: 446-460.